

Implications of the cosmic infrared background for light production and the star formation history in the Universe[★]

R. Gispert^{†**}, G. Lagache, and J.L. Puget

Université Paris XI, Institut d'Astrophysique Spatiale, Bâtiment 121, 91405 Orsay Cedex, France

Received 24 November 1999 / Accepted 16 May 2000

Abstract. The Cosmic Background due to the integrated radiation from galaxies over the whole life of the Universe is reviewed. We find that this background is well constrained by measurements. The total power in the background is in the range 60–93 nWm⁻²sr⁻¹. The data show the existence of a minimum separating the direct stellar radiation from the infrared part due to radiation reemitted by dust. This reemitted dust radiation is about 1–2.6 time the background power in the optical/near-IR thus much larger than the same ratio measured locally (30%). The far-infrared and submillimeter background is likely to be dominated by redshifted infrared galaxies. The long wavelength spectrum of the background being significantly flatter than the spectrum of these galaxies it strongly constrains the far-infrared radiation production rate history which must increase by a factor larger than 10 between the present time and a redshift 1 and then stays rather constant at higher redshift, contrary to the ultraviolet radiation production rate which decreases rapidly.

Several models of galaxy evolution have been proposed to explain the submillimeter background. In this paper we do not propose a new model; we systematically explore the allowed range of evolution histories allowed by the data. If infrared galaxies are mostly powered by starbursts as indicated by recent observations, this infrared production history reflects the history of starformation in the Universe.

Key words: cosmology: observations – cosmology: diffuse radiation – infrared: galaxies

1. Introduction

The history of star formation in the Universe is one of the key function in physical cosmology. It is closely linked to galaxy formation and evolution and controls the second most important contribution to the cosmic electromagnetic background after the Cosmic Microwave Background (CMB) generated at the time of recombination at a redshift around 1000. It has been pointed

out many times in the past 30 years, that measurements of the cosmic background radiated by all galaxies over the history of the Universe would be extremely valuable for physical cosmology. It would strongly constrain models for galaxy formation and evolution (see for example Partridge & Peebles 1967). This background is expected to be composed of three main components:

- The stellar radiation in galaxies concentrated in the ultraviolet and visible with a redshifted component in the near InfraRed (IR)
- A fraction of the stellar radiation absorbed by dust either in the galaxies or in the intergalactic medium
- The radiation from active galactic nuclei (a fraction of which is also absorbed by dust and reradiated in the far-IR).

The energy in the first two components is derived from nucleosynthesis in stars, the last one probably derived from gravitational energy of accreted matter onto massive black holes. In the last two years the cosmic background at visible, IR and submillimeter (submm) wavelengths has been finally constrained by very deep source counts and upper limits on the diffuse isotropic emission at shorter wavelengths, and measured in the submm range. We review the observational situation in Sect. 2. In Sect. 3, we define the formalism of the determination of the IR radiation production rate history. When the spectrum of the sources dominating the background is strongly peaked around a wavelength of 80 μm, the radiation production rate as a function of redshift can be directly inferred from the spectrum of the cosmic background. In Sect. 4, the sources of Cosmic Far-IR BackgRound (CFIRB) and their spectra are reviewed. In the likely hypothesis of this background being dominated by IR galaxies (either starburst galaxies or dust enshrouded AGNs), we derive the IR radiation production rate as a function of redshift in the Universe (Sect. 5). We compare it with other means to measure the star formation rate in Sect. 6.

The study presented here is different from the many studies of this type based on a model for Spectral Energy Distribution (SED) and evolution of IR galaxies which, after some adjustments, account for the Cosmic Background. Considering the diversity of SED which can be used and the observational uncertainties it is clear that a range of histories of the IR galaxies is possible. The goal of this paper and of the method presented

Send offprint requests to: G. Lagache (lagache@ias.fr)

[★] Appendix 1 and 2 are only available electronically with the On-Line publication at <http://link.springer.de/link/service/00230/>

^{**} Richard Gispert died in the final stages of the preparation of this paper in August 1999.

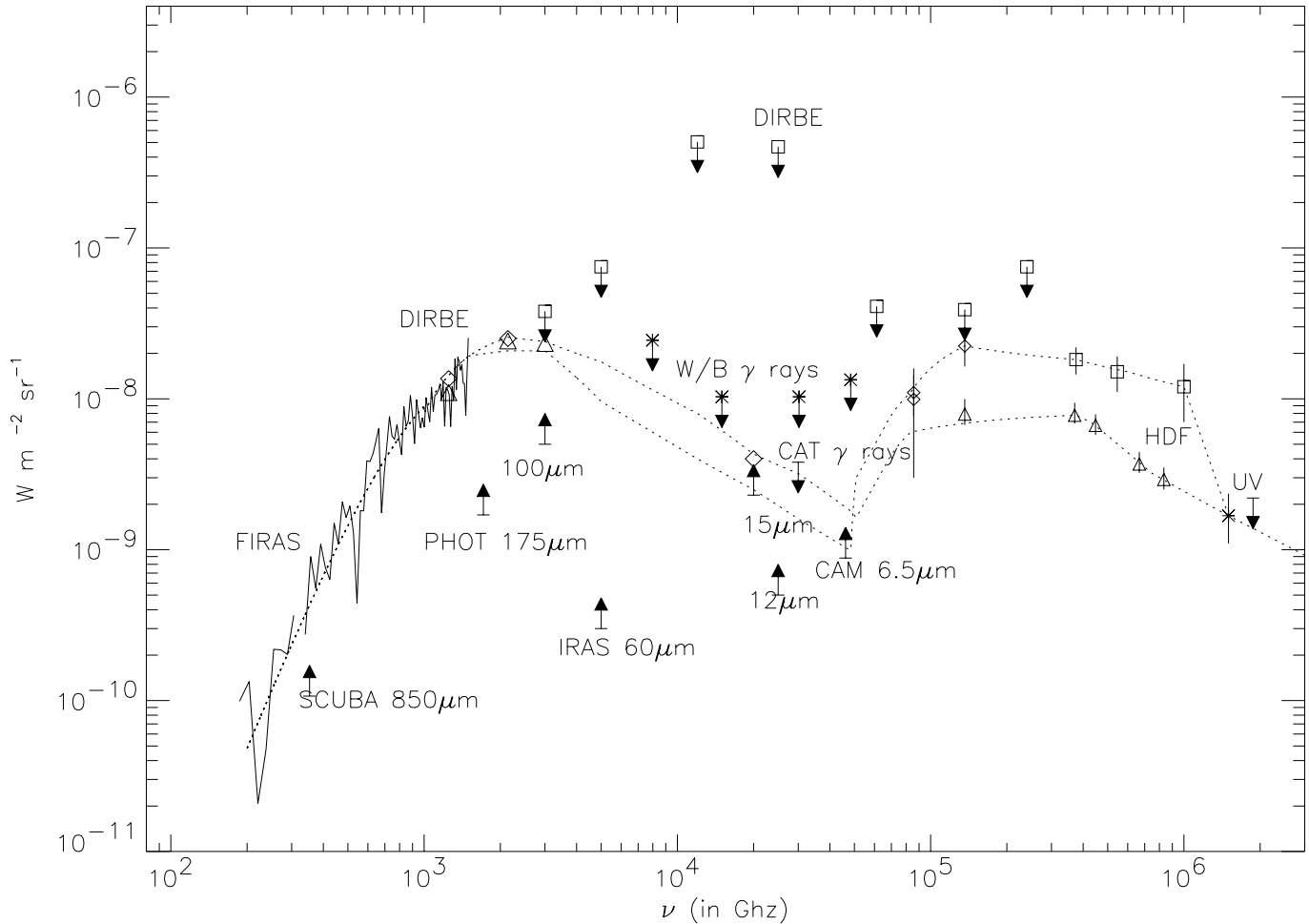


Fig. 1. Cosmic Background from the UV to the millimeter wavelength. In the UV domain, the upper limit is from Martin et al. (1991) and the value from Armand et al. (1994); the optical and near-IR points are from Pozzetti et al. (1998) (triangles) and Bernstein et al., in preparation (squares); The 3.5 and 2.2 μm points are from Dwek & Arendt (1998) and Gorjian et al. (2000); Squared upper limits are from Hauser et al. (1998) and crossed upper limits from Biller et al. (1998); the upper limit “CAT” is from Barrau (1998) and Barrau et al., in preparation; The 6.5 (Désert, private communication), 12 (Clements et al. 1999) and 15 μm (Elbaz et al. 1999) lower limits come from ISOCAM number counts; the value at 15 μm (\diamond) is an extrapolation of the counts using the Guiderdoni et al. (1998) model. At longer wavelength, we have the 100, 140 and 240 μm Lagache et al. (2000) (\triangle) and Hauser et al. (1998) (\diamond) DIRBE values, lower limit from Dwek et al. (1998), upper limits from number counts at 60 (Lonsdale et al. 1990), 175 (Puget et al. 1999) and 850 μm (Barger et al. 1999). Dotted lines are an attempt to draw continuous lines compatible with all available data which then can be used for estimating the energy contribution of a given wavelength range.

here is to explore systematically the range of possible solutions by a careful analysis of possible SEDs taking properly into account the observational uncertainties. The method developed in this paper is the only one so far to answer this question.

2. The Cosmic Background Radiation: observations

We summarise here the observational situation of the cosmic background which is the main observation used in this study. The values of the cosmic background at all wavelengths are discussed in Appendix A and shown in Fig. 1. We can compute the energy contained in the background above and below 6 μm using the best fits presented in Fig. 1. We obtain:

- $E(<6 \mu\text{m})=E(\text{opt})= 2\text{-}4.1 \cdot 10^{-8} \text{ W m}^{-2} \text{ sr}^{-1}$
- $E(>6 \mu\text{m})=E(\text{FIR})= 4\text{-}5.2 \cdot 10^{-8} \text{ W m}^{-2} \text{ sr}^{-1}$.

We know that for local galaxies the ratio $E(\text{FIR})/E(\text{opt})$ is about 0.3 (Soifer & Neugebauer 1991). We measure here a higher ratio which is about 1-2.6. This higher ratio results from two combined effects. First, the redshift effect will bring the light from optical to IR and thus will give more energy in the IR than for local galaxies. Nevertheless this effect cannot account for an IR to optical ratio much larger on average than the value observed today. This higher ratio can only be explained by a change of properties of galaxies that are making the background in the optical and the IR. A very simple comparison supports this idea: the energy in the background at 15 μm and in the optical domain is nearly the same. But the background at 15 μm in the Hubble Deep Field is made by a very small number of objects as compared to the number of sources which contribute to the bulk of the energy observed in the optical (Aussel et al. 1999).

This means that the background in the IR is probably dominated by few objects with high IR luminosities. Thus these objects are not the standard IR counterparts of normal spiral and irregular galaxies.

3. Formalism of the determination of the radiation production rate history in the Universe

For a Universe following a Robertson-Walker metric with total density Ω_0 , and a cosmological constant Ω_Λ , the differential contribution dE to the background energy density (monochromatic or integrated over frequency, per unit volume) generated around redshift z during time dt is:

$$dE = \frac{\varphi(z)}{(1+z)} dt \quad (1)$$

where φ is the comoving energy production rate per unit volume at redshift z (note that here φ is not the spectral energy density).

The background spectral intensity (brightness per solid angle and frequency interval) I_ν is such that:

$$\nu I_\nu = \frac{c}{4\pi} \varphi(z) \left| \frac{dt}{dz} \right|_{1+z=\frac{\nu'}{\nu}} \quad (2)$$

where we assume a monochromatic spectrum for the sources radiating at frequency $\nu' = \nu(1+z)$ where ν is the observed frequency. In that case (δ function spectrum for the emitting objects), $\varphi(z)$ can be simply deduced from the background spectrum νI_ν (see Appendix B).

The relations given above can be easily generalised to the case where the sources radiate through a broad spectrum:

$$\nu I_\nu = \frac{c\nu}{4\pi} \int_{\nu'=\nu}^{\infty} N_z L_{\nu'} \left| \frac{dt}{dz} \right| d\nu' \quad (3)$$

with N_z the number of sources per Mpc^3 and $L_{\nu'}$ the luminosity of the galaxies (in W/Hz).

$L_{\nu'}$ is the average over a large volume of SED of luminous IR galaxies which have been shown to dominate the $15 \mu\text{m}$ background at $z \simeq 0.7$ (Aussel et al. 1999). The range of SED for IR galaxies are discussed in Sect. 4. The important result of this discussion is that all the far-IR SEDs of luminous IR galaxies are not very dependent of the energy source (starburst or dust enshrouded AGN) and varies slowly with the luminosity (Maffei 1994; Guiderdoni 1998).

The unknown quantity in Eq. (3) becomes N_z . The full range of allowed functions for the number density of sources as a function of z is derived using Monte Carlo simulations for a set of IR galaxy spectra which covers the range of possible ones and for different cosmological models. The number density multiplied by the total luminosity of each model galaxy gives the IR luminosity density φ in function of z :

$$\varphi(z) = N_z \int_{\nu_0} L_{\nu_0} d\nu_0 \quad (4)$$

$\varphi(z)$ depends on the cosmological model via the $\frac{dt}{dz}$.

¹ We can note that $\varphi(z) \times \frac{dt}{dz}$ is independent of the cosmological model. We nevertheless choose to use $\varphi(z)$ rather $\varphi(z) \times \frac{dt}{dz}$ as $\varphi(z)$ corresponds at $z=0$ to a measured value.

4. Sources of the Cosmic Background and their spectra

To determine $\varphi(z)$, we need to establish the range of acceptable average SEDs ($L_{\nu'}$) of the sources that are making the background.

Locally Soifer & Neugebauer (1991) have studied the population of IR galaxies at low redshift using the IRAS all sky survey. They have established the integrated IR luminosity per unit volume in the Universe today, its SED, the luminosity function of IR galaxies and the SED as a function of the integrated IR luminosity. The IR luminosity function shows two main components. One is associated with normal spiral galaxies which radiate a fraction of their energy in the IR (our Galaxy for example radiates about one third of its luminosity in the IR). These galaxies are expected to have a luminosity function similar to the luminosity function of galaxies in the optical. However, the IR luminosity function does not show an exponential cut off like optical galaxies but display a power law behaviour at high luminosities: $\frac{dN}{dL} = L^{-2}$. This is also shown by more recent compilations of the IR luminosity functions (Sanders & Mirabel 1996). This shows that the very luminous IR galaxies cannot be the IR counterpart of optical galaxies. In fact they have been shown to be starburst galaxies often associated with merging or interacting systems and for which the ratio of IR to optical luminosity increases with the bolometric luminosity (Sanders & Mirabel 1996; Fang et al. 1998). One can thus conjecture that the luminosity function of mergers and interacting galaxies is very different from the luminosity function of normal galaxies. Using this rough separation, locally the relative contributions of starburst to normal galaxies is less than 10%. The integrated luminosity of normal galaxies is dominated by L_* optical galaxies ($L_{IR*} \simeq 10^{10} L_\odot$) whereas the integrated luminosity of IR starburst is dominated by galaxies with $L_{IR} \sim 10^{11} L_\odot$ (see for example Sanders & Mirabel 1996).

26 of the galaxy detected by ISOCAM in the HDF north are identified with galaxies with known redshifts. Aussel (1999) has shown that the IR galaxies have luminosities greater than $3 \cdot 10^{10} L_\odot$ at $8.5 \mu\text{m}$ (in the rest frame) with a median redshift of 0.75, and thus bolometric luminosities between 1 and $3 \cdot 10^{11} L_\odot$. These galaxies, identified mostly as interacting systems or spiral galaxies, are luminous IR galaxies undergoing a starburst phase.

Spectra of IR galaxies have been modeled by Maffei (1994), using the observational correlation of the IRAS flux ratio 12/60, 25/60 and 60/100 with the IR luminosity (Soifer & Neugebauer 1991). Examples of spectra for three different luminosities are shown in Fig. 2. The luminous IR galaxies are emitting more than 95% of their energy in the far-IR. Taking only such kind of galaxies obviously fails to reproduce the optical Extragalactic Background (EB). That is why we concentrate hereafter only on the far-IR part of the EB (the so-called Cosmic Far-IR Background, CFIRB).

It is possible however that part of the CFIRB energy might be due to dust enshrouded Active Galactic Nuclei (AGNs) for which the far-IR SED is very similar to starburst galaxies of similar luminosity. Based on the assumptions that 10% of the mass accreting into black hole is turned into energy and that the black

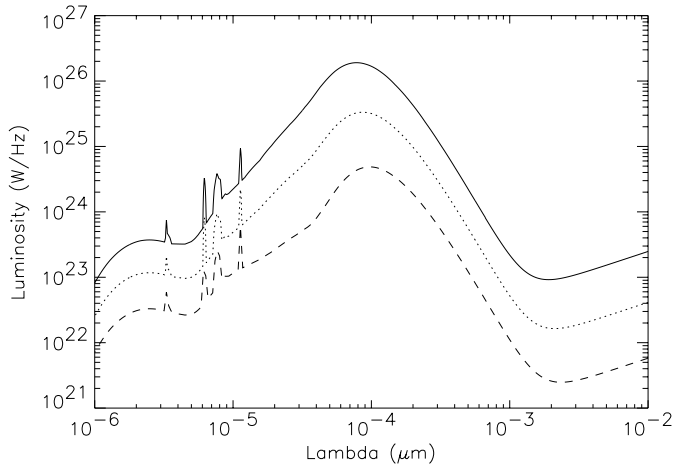


Fig. 2. Typical spectra of starburst galaxies (Maffei 1994) for different luminosities (continuous line: $3 \cdot 10^{12} L_{\odot}$, dotted line: $5 \cdot 10^{11} L_{\odot}$, dashed line: $7 \cdot 10^{10} L_{\odot}$) with a spectral dust emission index in the far-IR of 2.

hole masses measured in the HDF (Ford et al. 1998) are typical of galaxies, the AGN background energy would be in order of 10% of that from stars (Eales et al. 1999). These calculations are highly uncertain but are supported by the recent work of Almaini et al. (1999). The SEDs of high-redshift dust enshrouded AGNs are similar to those observed locally, and one can explain 10-20 % of the CFIRB. Because of the similar far-IR SEDs, the question of the fraction of the CFIRB due to AGNs is not relevant to the determination of the IR radiation production history. The estimates mentioned above are only important because they indicate that the IR radiation production history is likely to reflect the star formation history. Locally the average far-IR SED adjusted on the IRAS data (Soifer & Neugebauer 1991) is well represented by the SED of a $8 \cdot 10^{10} L_{\odot}$ galaxy. As we have seen, at $z \sim 0.7$ the mid IR production is dominated by galaxies typically 2.5 times more luminous. Finally at higher redshift the main indication comes from the SCUBA deep surveys and also indicates an average SED dominated by ultraluminous IR galaxies. To take into account the uncertainty on the average far-IR SED, we use for the determination of the IR radiation production history, the SEDs from Maffei (1994) for galaxies with luminosities $7 \cdot 10^{10} L_{\odot}$, $5 \cdot 10^{11} L_{\odot}$ and $3 \cdot 10^{12} L_{\odot}$ which takes into account the change in the peak emission wavelength with luminosity. For the long wavelength behaviour, we allow the dust emissivity index of the model to vary from 1.3 to 2 which covers generously the uncertainty on this parameter for the average SED.

5. Luminosity density history from Monte Carlo simulations

5.1. The CFIRB spectrum

We used the CFIRB determination as described in Lagache et al. (2000). The CFIRB resulting from an integral over a significant redshift range is expected to be a smooth function of frequency. Therefore, we use a smooth fit for the determination of $\varphi(z)$.

The CFIRB spectrum, can be fitted between 200 and 2000 μm by a modified Planck function as given by:

$$I(\nu) = 8.80 \times 10^{-5} (\nu/\nu_0)^{1.4} P_{\nu}(13.6K) \quad (5)$$

where $\nu_0 = 100 \text{ cm}^{-1}$. The set of parameters (T, τ, α) has been determined by a χ^2 minimization. The spectrum is sampled at 10 FIRAS frequency. The uncertainties on each sampled frequency are obtained by varying parameters until χ^2 is increased by 10%. In addition to the FIRAS data, we have used the CFIRB DIRBE determinations at 100, 140 and 240 μm (Lagache et al. 2000). CFIRB data points and uncertainties that are used for the determination of $\varphi(z)$ are shown in Fig. 5.

5.2. Determination of $\varphi(z)$

We determine the range of functions $\varphi(z)$ allowed by the data for each combination of SED and cosmological model. The cases used are given by the combinations of:

- Three IR galaxy luminosities ($3 \cdot 10^{12} L_{\odot}$, $5 \cdot 10^{11} L_{\odot}$ and $7 \cdot 10^{10} L_{\odot}$, see Fig. 2)
- Four values for the dust spectral index (1.3, 1.5, 1.7 and 2)
- Three cosmological models defined by the set of parameters h, Ω_0 and Ω_{Λ} ($h=0.65, \Omega_0=0.3, \Omega_{\Lambda}=0.7$; $h=0.65, \Omega_0=0.3, \Omega_{\Lambda}=0$, and $h=0.65, \Omega_0=1, \Omega_{\Lambda}=0$) which fix dt/dz .

To establish $\varphi(z)$ and the associated error bars we use Eq. (3). The basic algorithm for finding N_z is based on Monte Carlo simulations. N_z is sampled at a few redshift values and linearly interpolated between these values for computing the term on the right side of Eq. (3). It has been assumed that beyond $z=13$, $N_z=0$. For each case, the solution (minimum χ^2) has been obtained by exploring a wide range of randomly distributed values of N_z at each of the sampled values of z . Error bars are estimated by keeping the computed CFIRB within the uncertainties at each sampled frequency (see Fig. 5) and greater than the lower CFIRB limit at 850 μm from Barger et al. (1999). By using an iterative method for progressively reducing the range of explored values, we reach convergence for each case studied with a reasonable number of hits (~ 50000). At $z=0$, the IR production rate in the Universe is around $1.65 \cdot 10^8 h L_{\odot}/\text{Mpc}^3$ (Soifer & Neugebauer 1991), where h is the Hubble constant in units of 100 km/sec/Mpc³. This gives $\varphi(z=0) = 10^8 L_{\odot}/\text{Mpc}^3$ for $h=0.65$.

5.3. Results

The results² are summarised in Table 1 for the different cosmologies and SEDs. We see that for all the considered cases, the χ^2 is very similar. This shows that, as expected, there is not a unique solution for the inversion in terms of cosmological model and average SEDs. Nevertheless the remarkable result is that there is a range of redshifts in which all acceptable solutions have the same behaviour as can be seen in Fig. 3 where the luminosity density variation, together with its uncertainties allowed

² Figures and results can be found on G. Lagache's WEB page: <http://www.ias.fr/iasnv/people.html>

Table 1. Co-moving luminosity density φ derived from the CFIRB for the three galaxy model luminosities, the four dust spectral indexes and the three cosmologies (defined by Ω_Λ and Ω_0). Numbers on the right side of each row correspond to the minimal and maximal value of φ compatible with the CFIRB. The Hubble constant is the same for all cases ($h=0.65$). Given in column 10 is the χ^2 of the CFIRB “fit” derived from the luminosity density compared to the FIRAS and DIRBE measured values.

Log(L), α , Ω_Λ , Ω_0	Luminosity density φ (L_\odot/Mpc^3)							χ^2
	z=0.4	z=0.8	z=1.2	z=1.9	z=2.7	z=4.8	z=8	
12.5, 2.0, 0.0, 0.3	8.94 10 ^{8.28 10⁹} 8.28 10 ⁶	1.15 10 ^{9.145 10⁹} 6.75 10 ⁸	1.53 10 ^{9.208 10⁹} 1.04 10 ⁹	1.26 10 ^{9.185 10⁹} 8.61 10 ⁸	1.43 10 ^{9.195 10⁹} 7.76 10 ⁸	6.68 10 ^{8.123 10⁹} 6.68 10 ⁶	3.82 10 ^{8.707 10⁸} 4.13 10 ⁶	0.054
12.5, 2.0, 0.7, 0.3	6.36 10 ^{8.101 10¹⁰} 1.27 10 ⁷	1.54 10 ^{9.194 10⁹} 9.74 10 ⁸	1.91 10 ^{9.259 10⁹} 1.40 10 ⁹	1.86 10 ^{9.253 10⁹} 1.27 10 ⁹	2.01 10 ^{9.296 10⁹} 1.18 10 ⁹	1.14 10 ^{9.211 10⁹} 3.34 10 ⁷	5.64 10 ^{8.121 10⁹} 4.83 10 ⁶	0.053
12.5, 2.0, 0.0, 1.0	3.02 10 ^{8.820 10⁹} 1.77 10 ⁶	1.36 10 ^{9.185 10⁹} 8.60 10 ⁸	1.96 10 ^{9.267 10⁹} 1.24 10 ⁹	1.73 10 ^{9.254 10⁹} 1.18 10 ⁹	2.06 10 ^{9.281 10⁹} 1.12 10 ⁹	1.04 10 ^{9.207 10⁹} 1.04 10 ⁷	6.75 10 ^{8.125 10⁹} 6.75 10 ⁶	0.053
11.7, 2.0, 0.0, 0.3	1.50 10 ^{9.752 10⁹} 8.77 10 ⁶	1.37 10 ^{9.172 10⁹} 8.64 10 ⁸	1.49 10 ^{9.219 10⁹} 1.01 10 ⁹	1.17 10 ^{9.171 10⁹} 7.95 10 ⁸	1.25 10 ^{9.170 10⁹} 6.28 10 ⁸	4.15 10 ^{8.964 10⁸} 3.84 10 ⁶	3.82 10 ^{8.519 10⁸} 4.45 10 ⁶	0.057
11.7, 2.0, 0.7, 0.3	1.17 10 ^{9.957 10⁹} 7.85 10 ⁶	1.84 10 ^{9.239 10⁹} 1.24 10 ⁹	2.03 10 ^{9.264 10⁹} 1.37 10 ⁹	1.71 10 ^{9.222 10⁹} 1.15 10 ⁹	1.82 10 ^{9.237 10⁹} 9.42 10 ⁸	7.46 10 ^{8.164 10⁹} 5.73 10 ⁶	4.35 10 ^{8.839 10⁸} 4.35 10 ⁶	0.057
11.7, 2.0, 0.0, 1.0	5.24 10 ^{8.638 10⁹} 5.24 10 ⁶	1.75 10 ^{9.228 10⁹} 1.18 10 ⁹	1.96 10 ^{9.254 10⁹} 1.32 10 ⁹	1.65 10 ^{9.215 10⁹} 1.11 10 ⁹	1.79 10 ^{9.233 10⁹} 1.06 10 ⁹	7.34 10 ^{8.142 10⁹} 6.44 10 ⁶	4.62 10 ^{8.891 10⁸} 5.27 10 ⁶	0.056
10.8, 2.0, 0.0, 0.3	6.61 10 ^{8.567 10⁹} 6.12e+05	2.11 10 ^{9.266 10⁹} 1.33 10 ⁹	1.65 10 ^{9.242 10⁹} 9.64 10 ⁸	1.14 10 ^{9.168 10⁹} 7.78 10 ⁸	1.06 10 ^{9.144 10⁹} 5.74 10 ⁸	3.72 10 ^{8.801 10⁸} 3.72 10 ⁶	2.15 10 ^{8.397 10⁸} 2.32 10 ⁶	0.065
10.8, 2.0, 0.7, 0.3	7.88 10 ^{8.788 10⁹} 9.19 10 ⁶	2.69 10 ^{9.339 10⁹} 1.70 10 ⁹	2.26 10 ^{9.331 10⁹} 1.42 10 ⁹	1.61 10 ^{9.236 10⁹} 1.09 10 ⁹	1.56 10 ^{9.212 10⁹} 8.44 10 ⁸	5.62 10 ^{8.121 10⁹} 5.62 10 ⁶	3.65 10 ^{8.675 10⁸} 3.95 10 ⁶	0.065
10.8, 2.0, 0.0, 1.0	1.04 10 ^{9.574 10⁹} 7.98 10 ⁶	2.48 10 ^{9.323 10⁹} 1.67 10 ⁹	2.13 10 ^{9.277 10⁹} 1.44 10 ⁹	1.55 10 ^{9.231 10⁹} 1.05 10 ⁹	1.50 10 ^{9.196 10⁹} 7.79 10 ⁸	5.81 10 ^{8.112 10⁹} 5.81 10 ⁶	3.49 10 ^{8.674 10⁸} 4.54 10 ⁶	0.062
12.5, 1.7, 0.0, 0.3	9.48 10 ^{8.753 10⁹} 6.12e+05	1.29 10 ^{9.162 10⁹} 7.52 10 ⁸	1.52 10 ^{9.206 10⁹} 1.03 10 ⁹	1.27 10 ^{9.173 10⁹} 8.65 10 ⁸	1.30 10 ^{9.176 10⁹} 7.01 10 ⁸	4.92 10 ^{8.106 10⁹} 4.92 10 ⁶	3.32 10 ^{8.569 10⁸} 3.59 10 ⁶	0.054
12.5, 1.7, 0.7, 0.3	2.58 10 ^{9.120 10¹⁰} 6.00 10 ⁶	1.54 10 ^{9.210 10⁹} 9.02 10 ⁸	2.01 10 ^{9.273 10⁹} 1.37 10 ⁹	1.76 10 ^{9.258 10⁹} 1.11 10 ⁹	1.81 10 ^{9.266 10⁹} 9.79 10 ⁸	8.55 10 ^{8.171 10⁹} 8.55 10 ⁶	4.78 10 ^{8.953 10⁸} 4.42 10 ⁶	0.051
12.5, 1.7, 0.0, 1.0	4.31 10 ^{8.737 10⁹} 2.00 10 ⁷	1.54 10 ^{9.209 10⁹} 9.72 10 ⁸	2.02 10 ^{9.275 10⁹} 1.28 10 ⁹	1.72 10 ^{9.252 10⁹} 1.17 10 ⁹	1.86 10 ^{9.253 10⁹} 1.01 10 ⁹	8.18 10 ^{8.163 10⁹} 8.18 10 ⁶	5.25 10 ^{8.971 10⁸} 5.25 10 ⁶	0.054
11.7, 1.7, 0.0, 0.3	1.03 10 ^{9.651 10⁹} 7.59 10 ⁶	1.60 10 ^{9.201 10⁹} 1.01 10 ⁹	1.59 10 ^{9.216 10⁹} 1.00 10 ⁹	1.17 10 ^{9.172 10⁹} 7.98 10 ⁸	1.11 10 ^{9.151 10⁹} 5.99 10 ⁸	3.78 10 ^{8.814 10⁸} 3.50 10 ⁶	2.69 10 ^{8.426 10⁸} 3.65 10 ⁶	0.060
11.7, 1.7, 0.7, 0.3	8.92 10 ^{8.835 10⁹} 6.01 10 ⁶	2.11 10 ^{9.275 10⁹} 1.43 10 ⁹	2.12 10 ^{9.275 10⁹} 1.43 10 ⁹	1.64 10 ^{9.214 10⁹} 1.11 10 ⁹	1.61 10 ^{9.210 10⁹} 8.36 10 ⁸	6.37 10 ^{8.123 10⁹} 6.37 10 ⁶	3.82 10 ^{8.738 10⁸} 4.36 10 ⁶	0.059
11.7, 1.7, 0.0, 1.0	1.22 10 ^{9.677 10⁹} 9.41 10 ⁶	1.90 10 ^{9.247 10⁹} 1.12 10 ⁹	2.03 10 ^{9.264 10⁹} 1.37 10 ⁹	1.60 10 ^{9.208 10⁹} 1.08 10 ⁹	1.61 10 ^{9.209 10⁹} 8.33 10 ⁸	6.07 10 ^{8.134 10⁹} 6.07 10 ⁶	4.21 10 ^{8.713 10⁸} 4.80 10 ⁶	0.057
10.8, 1.7, 0.0, 0.3	8.92 10 ^{8.563 10⁹} 8.27 10 ⁶	2.43 10 ^{9.305 10⁹} 1.53 10 ⁹	1.71 10 ^{9.270 10⁹} 9.24 10 ⁸	1.13 10 ^{9.166 10⁹} 7.71 10 ⁸	9.98 10 ^{8.136 10⁹} 5.40 10 ⁸	3.17 10 ^{8.683 10⁸} 2.00 10 ⁶	1.72 10 ^{8.317 10⁸} 2.00 10 ⁶	0.069
10.8, 1.7, 0.7, 0.3	2.28 10 ^{9.840 10⁹} 1.55 10 ⁷	2.77 10 ^{9.377 10⁹} 1.75 10 ⁹	2.45 10 ^{9.360 10⁹} 1.43 10 ⁹	1.50 10 ^{9.238 10⁹} 1.02 10 ⁹	1.40 10 ^{9.190 10⁹} 7.57 10 ⁸	5.11 10 ^{8.110 10⁹} 5.11 10 ⁶	2.90 10 ^{8.535 10⁸} 2.90 10 ⁶	0.065
10.8, 1.7, 0.0, 1.0	1.06 10 ^{9.573 10⁹} 9.80 10 ⁶	2.86 10 ^{9.360 10⁹} 1.81 10 ⁹	2.27 10 ^{9.333 10⁹} 1.32 10 ⁹	1.54 10 ^{9.226 10⁹} 1.05 10 ⁹	1.41 10 ^{9.191 10⁹} 7.61 10 ⁸	4.90 10 ^{8.106 10⁹} 4.54 10 ⁶	3.07 10 ^{8.526 10⁸} 3.87 10 ⁶	0.066
12.5, 1.5, 0.0, 0.3	1.31 10 ^{9.765 10⁹} 7.09 10 ⁶	1.25 10 ^{9.170 10⁹} 7.88 10 ⁸	1.62 10 ^{9.220 10⁹} 1.02 10 ⁹	1.24 10 ^{9.181 10⁹} 8.42 10 ⁸	1.19 10 ^{9.175 10⁹} 6.44 10 ⁸	4.28 10 ^{8.922 10⁸} 3.96 10 ⁶	3.13 10 ^{8.460 10⁸} 3.65 10 ⁶	0.058
12.5, 1.5, 0.7, 0.3	8.95 10 ^{8.838 10⁹} 7.84 10 ⁶	1.82 10 ^{9.237 10⁹} 1.23 10 ⁹	2.09 10 ^{9.271 10⁹} 1.41 10 ⁹	1.70 10 ^{9.221 10⁹} 1.14 10 ⁹	1.86 10 ^{9.242 10⁹} 9.64 10 ⁸	6.58 10 ^{8.145 10⁹} 5.77 10 ⁶	4.90 10 ^{8.829 10⁸} 4.90 10 ⁶	0.057
12.5, 1.5, 0.0, 1.0	5.64 10 ^{8.602 10⁹} 8.36 10 ⁶	1.73 10 ^{9.225 10⁹} 1.02 10 ⁹	1.99 10 ^{9.259 10⁹} 1.34 10 ⁹	1.66 10 ^{9.246 10⁹} 1.12 10 ⁹	1.77 10 ^{9.230 10⁹} 1.04 10 ⁹	7.22 10 ^{8.139 10⁹} 6.33 10 ⁶	4.60 10 ^{8.779 10⁸} 5.25 10 ⁶	0.056
11.7, 1.5, 0.0, 0.3	1.26 10 ^{9.586 10⁹} 7.97 10 ⁶	1.68 10 ^{9.212 10⁹} 1.06 10 ⁹	1.72 10 ^{9.252 10⁹} 1.00 10 ⁹	1.10 10 ^{9.174 10⁹} 8.06 10 ⁸	1.09 10 ^{9.149 10⁹} 5.49 10 ⁸	3.22 10 ^{8.748 10⁸} 2.76 10 ⁶	2.46 10 ^{8.361 10⁸} 2.65 10 ⁶	0.065
11.7, 1.5, 0.7, 0.3	1.35 10 ^{9.790 10⁹} 1.25 10 ⁷	2.28 10 ^{9.287 10⁹} 1.44 10 ⁹	2.19 10 ^{9.298 10⁹} 1.38 10 ⁹	1.59 10 ^{9.233 10⁹} 1.08 10 ⁹	1.55 10 ^{9.211 10⁹} 8.41 10 ⁸	5.50 10 ^{8.119 10⁹} 5.50 10 ⁶	3.52 10 ^{8.602 10⁸} 3.52 10 ⁶	0.061
11.7, 1.5, 0.0, 1.0	1.10 10 ^{9.691 10⁹} 7.38 10 ⁶	2.05 10 ^{9.266 10⁹} 1.38 10 ⁹	2.11 10 ^{9.274 10⁹} 1.42 10 ⁹	1.57 10 ^{9.234 10⁹} 1.06 10 ⁹	1.53 10 ^{9.200 10⁹} 7.95 10 ⁸	5.01 10 ^{8.110 10⁹} 5.71 10 ⁶	4.24 10 ^{8.629 10⁸} 4.24 10 ⁶	0.060
10.8, 1.5, 0.0, 0.3	1.40 10 ^{9.601 10⁹} 7.56 10 ⁶	2.60 10 ^{9.327 10⁹} 1.52 10 ⁹	1.79 10 ^{9.284 10⁹} 9.69 10 ⁸	1.07 10 ^{9.170 10⁹} 7.32 10 ⁸	9.61 10 ^{8.131 10⁹} 4.82 10 ⁸	2.62 10 ^{8.609 10⁸} 2.25 10 ⁶	1.81 10 ^{8.287 10⁸} 2.28 10 ⁶	0.070
10.8, 1.5, 0.7, 0.3	1.08 10 ^{9.733 10⁹} 9.96 10 ⁶	3.40 10 ^{9.428 10⁹} 2.14 10 ⁹	2.53 10 ^{9.372 10⁹} 1.48 10 ⁹	1.59 10 ^{9.234 10⁹} 1.08 10 ⁹	1.37 10 ^{9.187 10⁹} 7.43 10 ⁸	4.54 10 ^{8.978 10⁸} 4.21 10 ⁶	2.77 10 ^{8.474 10⁸} 3.23 10 ⁶	0.071
10.8, 1.5, 0.0, 1.0	1.03 10 ^{9.558 10⁹} 9.54 10 ⁶	3.16 10 ^{9.398 10⁹} 1.99 10 ⁹	2.39 10 ^{9.351 10⁹} 1.40 10 ⁹	1.53 10 ^{9.225 10⁹} 1.04 10 ⁹	1.38 10 ^{9.187 10⁹} 6.90 10 ⁸	4.26 10 ^{8.918 10⁸} 3.95 10 ⁶	2.91 10 ^{8.462 10⁸} 3.15 10 ⁶	0.069
12.5, 1.3, 0.0, 0.3	1.69 10 ^{9.785 10⁹} 1.24 10 ⁷	1.39 10 ^{9.189 10⁹} 8.14 10 ⁸	1.57 10 ^{9.231 10⁹} 9.91 10 ⁸	1.20 10 ^{9.176 10⁹} 7.56 10 ⁸	1.16 10 ^{9.158 10⁹} 5.81 10 ⁸	3.86 10 ^{8.832 10⁸} 3.86 10 ⁶	2.07 10 ^{8.412 10⁸} 2.41 10 ⁶	0.057
12.5, 1.3, 0.7, 0.3	1.16 10 ^{9.834 10⁹} 6.84 10 ⁶	1.93 10 ^{9.251 10⁹} 1.30 10 ⁹	2.14 10 ^{9.278 10⁹} 1.44 10 ⁹	1.69 10 ^{9.220 10⁹} 1.14 10 ⁹	1.67 10 ^{9.217 10⁹} 8.63 10 ⁸	6.12 10 ^{8.135 10⁹} 6.12 10 ⁶	4.03 10 ^{8.682 10⁸} 4.59 10 ⁶	0.057
12.5, 1.3, 0.0, 1.0	1.23 10 ^{9.732 10⁹} 8.70 10 ⁶	1.76 10 ^{9.235 10⁹} 1.05 10 ⁹	2.07 10 ^{9.277 10⁹} 1.39 10 ⁹	1.61 10 ^{9.228 10⁹} 1.08 10 ⁹	1.66 10 ^{9.235 10⁹} 8.82 10 ⁸	5.52 10 ^{8.124 10⁹} 5.21 10 ⁶	4.70 10 ^{8.663 10⁸} 5.58 10 ⁶	0.056
11.7, 1.3, 0.0, 0.3	1.57 10 ^{9.730 10⁹} 6.26 10 ⁶	1.76 10 ^{9.239 10⁹} 1.11 10 ⁹	1.73 10 ^{9.254 10⁹} 1.01 10 ⁹	1.13 10 ^{9.165 10⁹} 7.67 10 ⁸	9.44 10 ^{8.139 10⁹} 5.11 10 ⁸	3.29 10 ^{8.710 10⁸} 4.15 10 ⁶	1.79 10 ^{8.306 10⁸} 1.93 10 ⁶	0.063
11.7, 1.3, 0.7, 0.3	1.42 10 ^{9.830 10⁹} 1.32 10 ⁷	2.46 10 ^{9.310 10⁹} 1.55 10 ⁹	2.32 10 ^{9.315 10⁹} 1.46 10 ⁹	1.57 10 ^{9.231 10⁹} 1.07 10 ⁹	1.49 10 ^{9.202 10⁹} 8.05 10 ⁸	4.87 10 ^{8.105 10⁹} 4.87 10 ⁶	3.19 10 ^{8.546 10⁸} 2.96 10 ⁶	0.063
11.7, 1.3, 0.0, 1.0	1.28 10 ^{9.682 10⁹} 9.09 10 ⁶	2.23 10 ^{9.281 10⁹} 1.33 10<						

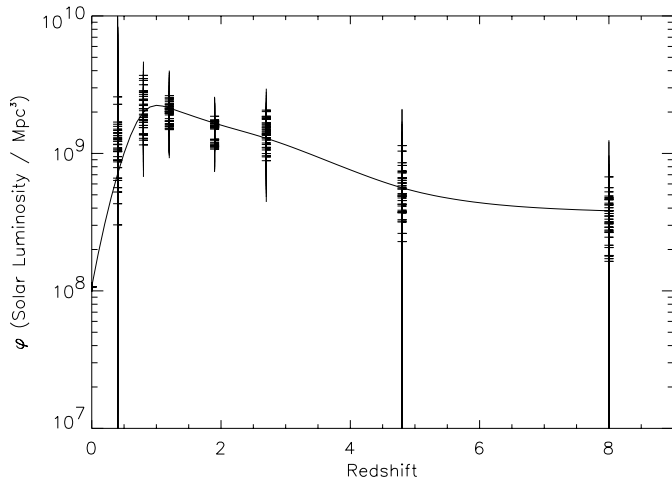


Fig. 3. Co-moving luminosity density distribution as derived from the CFIRB for all cases listed in Table 1. Also shown is the best fit passing through all cases.

by the data, is shown for each case. On the one hand, as could be expected, constraints on $\varphi(z)$ are very weak below redshift 1 (no cosmic background values at mid-IR wavelengths) and above redshift 4 (very low signal to noise ratio of the CFIRB spectrum above $800 \mu\text{m}$). On the other hand between redshifts 1 and 4, the CFIRB gives strong constraints on the history of the far-IR production rate which cannot be established from any of the present source surveys. The luminosity density is about 10 times higher at $z=1$ than at $z=0$ and it is nearly constant up to redshift 4. Because of this rather constant behaviour, the level is only weakly dependent on the galaxy model spectrum taken with different peak wavelength (see Fig. 4) as a change in the peak wavelength mainly shifts the function $\varphi(z)$ in z . Moreover, the luminosity density in the redshift range 1 to 4 is not affected by changing the far-IR dust spectral index from 1.3 to 2. In Fig. 5 is shown the CFIRB models induced from the luminosity density variation for the three luminosities and a fixed cosmology. For the far-IR part of the spectrum, the different luminosities give automatically good fits. This is not necessarily the case below $100 \mu\text{m}$ where the result is very dependent of the galaxy model spectrum. With the present observational constraints, the best fit is obtained for a luminosity of $5 \cdot 10^{11} L_{\odot}$. This is very consistent with typical luminosities of IR galaxies that are making the background at $15 \mu\text{m}$ (Aussel 1999).

6. Cosmological implications

6.1. The star formation history of the Universe

Many models describing the evolution of galaxies including their IR and submm emission have been published in the recent years. In this section, we discuss only empirical determinations of the SFR derived from different observations.

The history of the cosmic Star Formation Rate (SFR) can be derived from deep optical surveys assuming that (1) the stellar Initial Mass function (IMF) is universal, (2) the far-UV light is proportionnal to the SFR and (3) extinction is negligible. The

presence of dust which absorbs most of the UV starlight in starburst galaxies makes this last assumption highly questionable. The corrections needed to account for extinction are rather uncertain and there is much controversy about the value of this correction. Moreover, the SFR deduced from optical surveys can be underestimated if there is a significant population of objects so obscured that they are not detected in these surveys. A direct determination of the fraction of the stellar radiation reradiated by dust can be obtained from the IR/submm surveys if the dust enshrouded AGNs do not dominate. However, so far, the catalogues of faint submm sources with reliable redshifts are not large enough to reconstruct the history of the SFR (see Lilly et al. 1999 for a first attempt). We have shown that strong constraints can be provided by the CFIRB in the redshift range 1 to 4. It is particularly interesting to compare our determination with (1) the optically-derived SFR, corrected for extinction in the same redshift range and (2) the SFR inferred from SCUBA submm surveys. However, it is beyond the scope of this paper to discuss the cosmological implications in term of star formation. Detail discussions exist for example in Dwek et al. (1998), Pei et al. (1999), and Madau (1997).

Fig. 6 shows a compilation of the SFR derived from UV/Vis/Near-IR surveys, together with our determination of the far-IR radiation production rate history (through an interpolation). To compare the star formation rate with the luminosity density, we have to use a conversion factor. We take $\frac{SFR}{M_{\odot} \text{yr}^{-1}} = \frac{L_{IR}}{7.7 \cdot 10^9 L_{\odot}}$ (Guiderdoni et al. 1998, with a Salpeter IMF), conversion which is in good agreement with that derived from Scoville & Young (1983) and Thronson & Telesco (1986). The UV luminosity density in Fig. 6 has been corrected for extinction by Steidel et al. (1999). We see a very good agreement between the UV and far-IR luminosity density confirming the need for a very large extinction correction. This is a strong indication that the population of galaxies that are making the submm EB ($300\text{-}800 \mu\text{m}$) seems to be the same as the population detected by Steidel et al. (1999) in their surveys of Lyman-break galaxies. This would also imply that the population of objects so obscured that they are not detected in UV/opt/near-IR surveys cannot contribute for a large fraction of the luminosity density.

Submm EB deduced SFR can also be compared to SCUBA results. Several groups are now conducting deep and ultra-deep blank-field surveys (Barger et al. 1999; Hughes et al. 1998; Eales et al. 1999), that follow the first survey of Smail et al. (1997) who discover a population of luminous galaxies emitting at $850 \mu\text{m}$ amplified by lensing from foreground clusters. Two of these groups (Hughes et al. 1998; Barger et al. 1999) currently give estimates of the submm source SFR whereas Lilly et al. (1999) discuss its probable behaviour. Table 2 compares the SFR derived from the submm EB and the SCUBA determination. There is a very good agreement between the two although the SCUBA estimates should be interpreted with caution since only 20-25 % of the detected sources have secure identifications (Sanders 1999).

Fig. 5 shows that all galaxies that are contributing to most of the background at $850 \mu\text{m}$ cannot have a luminosity greater than $2\text{-}3 \cdot 10^{12} L_{\odot}$, standard luminosities of the current detected

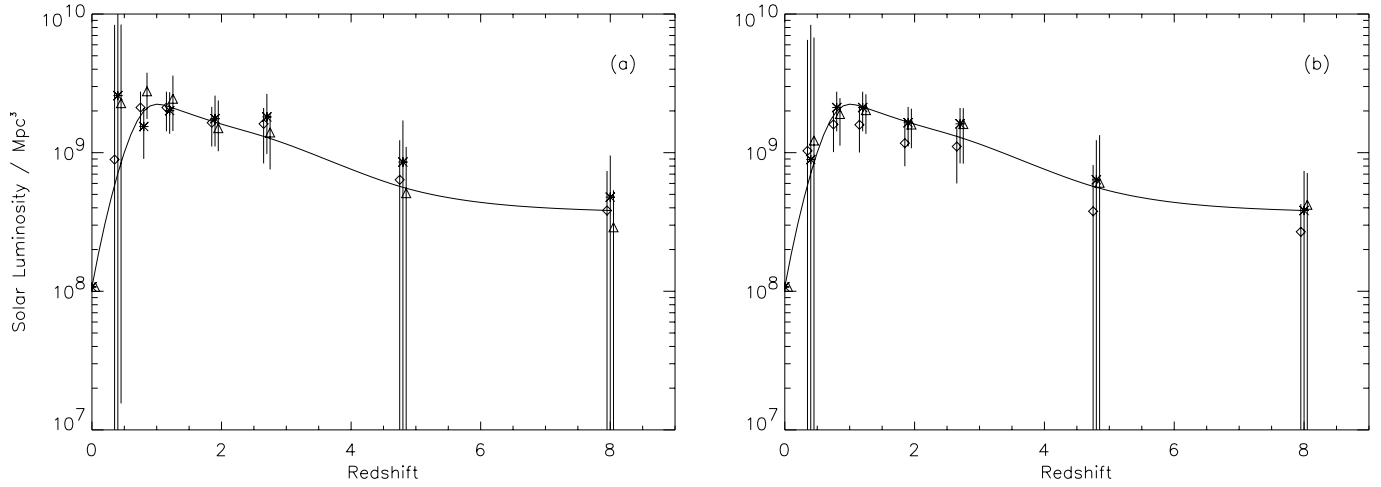


Fig. 4a and b. Co-moving luminosity density distribution as derived from the CFIRB for different sets of parameters (with a fixed dust spectral index of 1.7). **a:** for a given cosmological model ($\Omega_0=0.3$, $\Omega_\Lambda=0.7$) and different luminosities (star: $3 \cdot 10^{12} L_\odot$, diamond: $5 \cdot 10^{11} L_\odot$, triangle: $7 \cdot 10^{10} L_\odot$). **b:** given a luminosity of $5 \cdot 10^{11} L_\odot$ and three cosmological models with $h=0.65$ (star: $\Omega_0=0.3$, $\Omega_\Lambda=0.7$, diamond: $\Omega_0=0.3$, $\Omega_\Lambda=0$, triangle: $\Omega_0=1$, $\Omega_\Lambda=0$). In each plot, points around a redshift value have been arbitrarily shifted to see the uncertainties.

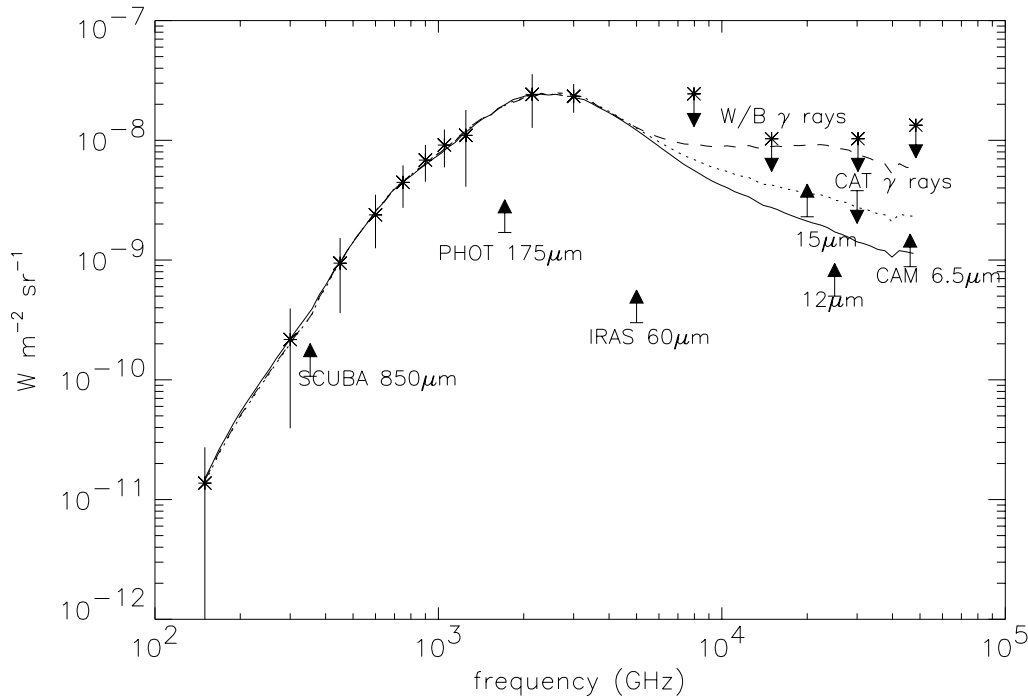


Fig. 5. CFIRB models induced from the luminosity density shown in Fig. 4a for the three luminosities (continuous line: $3 \cdot 10^{12} L_\odot$, dotted line: $5 \cdot 10^{11} L_\odot$, dashed line: $7 \cdot 10^{10} L_\odot$), a cosmology $h=0.65$, $\Omega_0=1$, $\Omega_\Lambda=0$. Also shown are the observational constraints and the CFIRB FIRAS and DIRBE spectrum (stars with error bars) computed as explained in Sect. 5.1.

Table 2. SFR (in $M_\odot \text{ yr}^{-1} \text{ Mpc}^{-3}$) deduced from the CFIRB and from deep submm SCUBA surveys (for $H_0=65 \text{ km s}^{-1} \text{ Mpc}^{-3}$).

Publications	Redshift	SFR
This paper	$z=1.9$	0.21 ± 0.10
Barger et al. 1999	$1 < z < 3$	0.25
Hughes et al. 1998	$2 < z < 4$	> 0.14

SCUBA sources (Lilly et al. 1999; Eales et al. 1999). This is consistent with the fact that SCUBA sources above 3 mJy account for only 20-30 % of the EB at $850 \mu\text{m}$. The present data show that the bulk of the submm EB is likely to reside in sources

with $850 \mu\text{m}$ fluxes near 1 mJy. Barger et al. (1999) estimate that the FIR luminosity of a characteristic 1 mJy source is in the range $4\text{-}5 \cdot 10^{11} L_\odot$, which is what is expected from Fig. 5.

It can be checked that models of galaxy evolution which fit the CFIRB fall within the allowed range of SFR histories obtained here (see for example Pei et al. 1999 and Guiderdoni et al. 1998).

6.2. Redshift contribution

In Fig. 7 is shown the relative contribution from different redshift ranges to the CFIRB as a function of wavelengths (for one

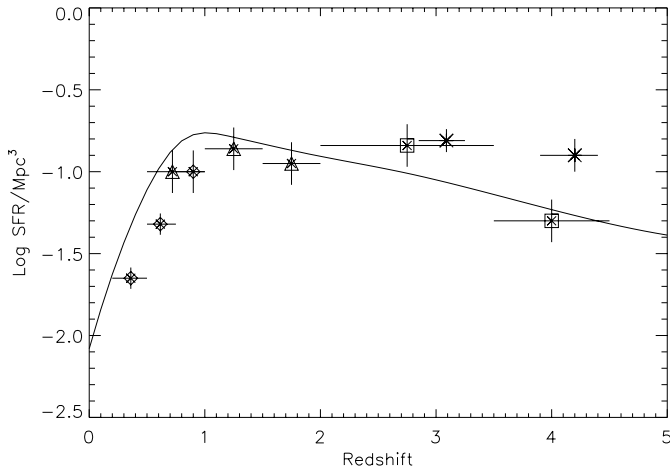


Fig. 6. SFR derived from UV/Vis/Near-IR observations (diamonds: Lilly et al. 1996; triangles: Conolly et al. 1997; squares: Madau et al. 1996; and crosses: Steidel et al. 1999) corrected for extinction by Steidel et al. (1999) and SFR derived from the CFIRB (continuous line, scaled to $H_0=50 \text{ km s}^{-1} \text{ Mpc}^{-1}$ for consistency)

illustrative case $\alpha=2$, $L=5 \cdot 10^{11} L_\odot$, $\Omega_0=0.3$ and $\Omega_\lambda=0.7$). As expected, galaxies below redshift 2.7 contribute mostly at short wavelengths and galaxies above redshift 2.7 contribute mostly at long wavelength. As can be seen in Fig. 4, the small error bar at $z \sim 2.5$ shows that this conclusion is firmly established. On the contrary, the fraction shown in Fig. 7 for redshift larger than 4.8 is not well constrained by the background.

At $850 \mu\text{m}$, about 20% of the CFIRB light comes from galaxies below redshift 2.7 and 80% from above. This can be compared with the recent results of Eales et al. (1999). Their data suggest that at least 15% of the $850 \mu\text{m}$ EB is emitted at $z < 3$, which is in good agreement with what we obtain here. However, our results show that a significant fraction of the submm EB comes from very distant objects. Such a scenario represents a picture in which a significant fraction of all stars has been formed very early in the Universe.

7. Summary

The CFIRB detected in the COBE data at wavelength greater than $100 \mu\text{m}$ contains a surprisingly large fraction of the cosmic background due to distant galaxies. The spectrum of this background at long wavelength is significantly flatter than the one observed for individual IR galaxies. This implies that the submm part of the CFIRB cannot be dominated by the emission of the galaxies which account for most of the CFIRB at $150 \mu\text{m}$, and thus contains a unique information about high redshift IR galaxies. Considering the variety of long wavelength spectra observed for these galaxies we have explored the range of possible redshift evolution histories. We show that only a co-moving production rate of far-IR radiation with strong evolution at low redshifts but little evolution between redshifts 1 and 4 is the only solution allowed by the CFIRB (the detailed low redshift evolution is much better constrained by the ISO deep surveys than by the background). Our results show that there is no evidence for

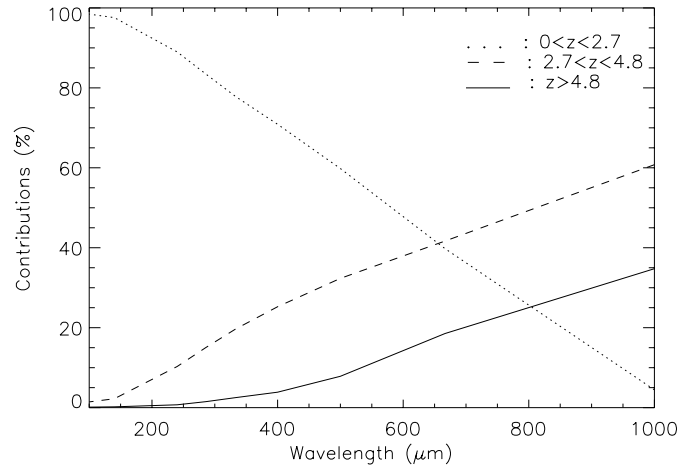


Fig. 7. Relative contribution to the CFIRB of galaxies with luminosity of $5 \cdot 10^{11} L_\odot$ for $z < 2.7$ (dotted line), $2.7 < z < 4.8$ (dashed line), and $z > 4.8$ (continuous line).

a “peak” in the cosmological star formation density at $z=1-2$ as it has been assumed by many authors; it is clear that the epoch of the beginning of star formation has not yet been identified. Moreover, these results indicate that there is a divergence of the behaviour of the star formation history as compared to that of the space density of luminous AGNs (see for example Dunlop 1997 and Shaver et al. 1998), as it was also suggested by Steidel et al. (1999).

Acknowledgements. We thank Martin Harwit for the discussions on the content of this paper. The work presented here profited from very useful comments from the referee E. Dwek.

References

- Almaini O., Lawrence A., Boyle B.J., 1999, MNRAS 305, 59
- Armand C., Milliard B., Deharveng J.M., 1994, A&A 284, 12
- Aussel H., 1999, PhD thesis, Paris VII University
- Aussel H., Cesarsky C.J., Elbaz D., Stark J.L., 1999, A&A 342, 313
- Barrau A., 1998, PhD thesis, Paris XI University
- Barger A.J., Cowie L.L., Sanders D.B., 1999, ApJ 518, L5
- Billier S.D., Buckley J., Burdett A., et al., 1998, Phys. Rev. Lett. 80, 2992
- Billier S.D., Akerlof C.W., Buckley J., et al., 1995, ApJ 445, 227
- Bowyer S., 1991, ARAA 29, 59
- Clements C., Désert F.X., Franceschini A., et al., 1999, A&A 346, 383
- Connolly A.J., Szalay A.S., Dickinson M., et al., 1997, ApJ 486, L11
- Dunlop J., 1997, In: Bremer M.N., Jackson N., Pérez-Fournon I. (eds.), Observational Cosmology with the New Radio Surveys (Kluwer: Dordrecht)
- Dwek E., Arendt R.G., 1998, ApJ 508, 9
- Dwek E., Arendt R.G., Hauser M.G., et al., 1998, ApJ 508, 106
- Eales S., Lilly S., Gear W.K.P., et al., 1999, ApJ 515, 518
- Elbaz D., Cesarsky C.J., Fadda D., et al., 1999, A&A 351, 37
- Fang F., Shupe D.L., Xu C., Hacking P.B., 1998, ApJ 500, 693
- Fixsen D.J., Dwek E., Mather J.C., et al., 1998, ApJ 508, 123
- Fixsen D.J., Cheng E.S., Cottingham D.A., et al., 1994, ApJ 420, 457
- Ford H.C., Tsvetanov Z.I., Ferrarese L., Jaffe, W., 1998, In: Sofue Y. (ed.) IAU Symp. 184, The Central Regions of the Galaxy and Galaxies (Kluwer: Dordrecht)

- Funk B., Magnussen N., Meyer H., et al., 1998, *Astroparticle Physics* 9, 97.
- Guiderdoni B., Hivon E., Bouchet F., Maffei B., 1998, *MNRAS* 295, 877
- Gorjian V., Wright E.L., Chary R.R., 2000, *ApJ* in press
- Hartmann D., 1994, Ph.D. thesis, University of Leiden
- Hauser M.G., Arendt R.G., Kelsall T., et al., 1998, *ApJ* 508, 25
- Hughes D., Serjeant S., Dunlop J., et al., 1998, *Nature* 394, 241
- Lagache G., Haffner L.M., Reynolds R.J., Tufte S.L., 2000, *A&A* 354, 247
- Lagache G., Abergel A., Boulager F., et al., 1999, *A&A* 344, 322
- Lilly S.J., Eales S.A., Gear W.K.P., et al., 1999, *ApJ* 518, 641
- Lilly S.J., Le Fèvre O., Hammer F., Crampton D., 1996, *ApJ* 460, L1
- Lonsdale C.J., Hacking P.B., Conrow T.P., Rowan-Robinson M., 1990, *ApJ* 358, 60
- Madau P., Pozzetti L., 2000, *MNRAS* 312, 9
- Madau P., Ferguson H., Dickinson M., et al., 1996, *MNRAS* 283, 1388
- Madau P., 1997, The evolution of luminous matter in the Universe, In: Livio M., Fall S.M., Madau P. (eds.) in "The Hubble deep field", STScI Symposium Series
- Maffei B., 1994, PhD thesis, Paris XI University
- Martin C., Hurwitz M., Bowyer S., 1991, *ApJ* 379, 549
- Mather J.C., Cheng E.S., Cottingham D.A., et al., 1994, *ApJ* 420, 439
- Milliard B., Donas J., Laget M., et al., 1992, *A&A* 257, 24
- Partridge R.B., Peeble P.J.E., 1967, *ApJ* 148, 377
- Pei Y.C., Fall S.M., Hauser M.G., 1999, *ApJ* 522, 604
- Pozzetti L., Madau P., Zamorani G., et al., 1998, *MNRAS* 298, 1133
- Puget J.L., Lagache G., Clements D.L. et al., 1999, *A&A* 354, 29
- Puget J.L., Abergel A., Bernard J.P., et al., 1996, *A&A* 308, L5
- Sanders D.B., 1999, In: Matsumoto T., de Graauw T. (eds.) *Space Infrared Telescopes and Related Science*, 32nd COSPAR workshop
- Sanders D.B., Mirabel I.F., 1996, *ARA&A* 34, 749
- Schlegel, D.J., Finkbeiner, D.P., Davis, M. 1998, *ApJ* 500, 525
- Scoville N.Z., Young J.S., 1983, *ApJ* 265, 148
- Shaver P.A., Hook I.M., Jackson C.A., et al., 1998, In: Carilli C., Radford S., Menten K., Langston G. (eds.) *Highly Redshifted Radio Lines*
- Smail I., Ivison R.J., Blain A.W., 1997, *ApJ* 490, L5
- Soifer B.T., Neugebauer G., 1991, *AJ* 101, 354
- Stecker F.W., De Jager O.C., 1993, *ApJ* 415, L71
- Steidel C.C., Adelberger K.L., Giavalisco M., et al., 1999, *ApJ* 519, 1
- Thronson H., Telesco C., 1986, *ApJ* 311, 98